

## Robustness of Interference Fractures that Promote Simultaneous Growth of Multiple Hydraulic Fractures

Peirce, A.P.

*University of British Columbia, Vancouver, BC, Canada*

Bunger, A.P.

*Department of Civil and Environmental Engineering, University of Pittsburgh, Pittsburgh, PA, USA*

Copyright 2014 ARMA, American Rock Mechanics Association

This paper was prepared for presentation at the 48<sup>th</sup> US Rock Mechanics / Geomechanics Symposium held in Minneapolis, MN, USA, 1-4 June 2014.

This paper was selected for presentation at the symposium by an ARMA Technical Program Committee based on a technical and critical review of

**ABSTRACT:** During horizontal well stimulation from an array of multiple perforations it is difficult to ensure simultaneous growth of all hydraulic fractures (HF) in the array due to a phenomenon known as stress shadowing, which favors the growth of the less constrained outer fractures in the array. Recently, using a fully coupled, parallel-planar 3D HF model it has been shown that it is possible to alleviate the localization effect of stress shadowing by appropriately breaking the symmetry of the perforation array. This procedure was termed interference fracturing due to the way in which the nearest neighbors to the outer fractures are positioned to interrupt the localization and runaway growth of the outer fractures. In this paper we will explore the robustness of the positioning of the interference fractures on a configuration designed to expose the changes to the dynamics of this complex fully-coupled system affected by perturbations to the initiation points in the array.

### 1. INTRODUCTION

There is considerable interest in being able to ensure the simultaneous growth of all hydraulic fractures from an array with multiple perforation clusters. If the perforations are sufficiently far apart then it is possible to obtain simultaneous growth from all the clusters in the array [1-2]. However, from a production standpoint it desirable to achieve a far greater density of perforations in an array than that which would guarantee a uniform simultaneous growth over all the fractures in the array. Unfortunately, when the perforation spacing is sufficiently small compared to the extent of the fractures, a phenomenon known as *stress shadowing* [3-7] occurs, one result of which is fracture growth that is localized to the outer two fractures in the array while the growth of the interior fractures in the array is severely stunted. Recently, using a parallel-planar HF model with full 3D elastic coupling between the simultaneously propagating fractures, it was shown [8] that it is possible to significantly reduce the stress shadow effect by the appropriate placement of *interference fractures* close to the outer fractures to inhibit their growth relative to the other fractures in the array.

In this paper, we explore the robustness of the interference fracture process by considering a numerical experiment having a one-parameter family of perforation

configurations. By sweeping through a range of values of the configuration parameter and monitoring various performance measures of the fracturing process, such as the total fractured area and the input energy cost, we explore the robustness of the interference fracturing process. In particular, we determine the value of the parameter that yields the optimal performance as well as the range of values in the neighborhood of this optimum over which significant performance gains can still be achieved.

The paper is organized as follows: in section 2 we provide a brief description of the numerical algorithm; in section 3 we provide illustrative examples of stress shadowing and interference fracturing for a uniform array and the optimal array respectively, in which the HF parameters such as input volume, elastic medium properties, and fluid viscosity are identical; in section 4 we provide the results of the numerical experiments; and in section 5 we provide some concluding remarks.

### 2. NUMERICAL MODEL

The numerical model used in this paper assumes that the fractures emanating from the multiple perforation clusters are constrained to grow in parallel planes (see Fig. 1), which are assumed to be perpendicular to the minimum principal stress direction.

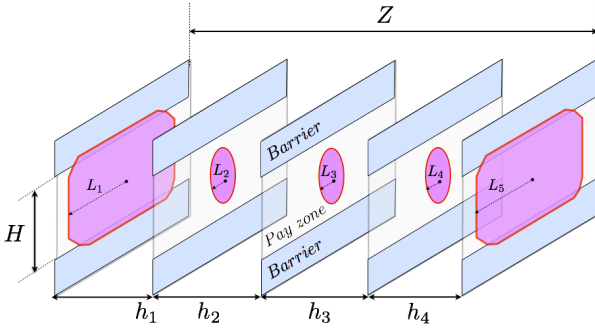


Fig. 1 Geometric configuration for the numerical model involving a perforation stage of length  $Z$  within a pay zone of height  $H$  in which  $h_k$  is the fracture spacing.

The elasto-static interaction between the multiple planar fractures is modeled by means of the displacement discontinuity method [9], in which each fracture plane is discretized into rectangular elements for which the crack opening field is assumed to be piecewise constant and quantities are collocated at element centers. The Reynolds lubrication equation, expressing the conservation of mass of the viscous fluid contained within the crack surfaces of each of the fractures, is discretized using a finite volume method, which is also defined with respect to quantities sampled at the centers of the rectangular elements. Similar to the volume of fluid approach, arbitrarily shaped fracture footprints are represented on this rectangular grid within each of these planes by introducing the notion of partially-filled crack tip elements. If the fracture front falls within a tip element, but does not encompass the center of the tip element itself, the fracture aperture field associated with the center of the element is still non-zero and represents the average volume of the crack opening that occurs within that tip element.

Since the majority of hydraulic fractures in the oil and gas industry are generated in high confinement reservoirs, it may be assumed that the fluid and the fracture fronts coalesce in which case the classic Stephan condition reduces to zero flux and width boundary conditions at the combined front [10]. In this case, a singularity in the pressure field at the fracture front typically occurs, whose strength depends on the regime of propagation [11]. We assume that the hydraulic fracture is propagating in the *viscosity regime*, in which the energy expended in viscous dissipation dominates the energy required to break the rock, which is related to the fracture toughness.

Because of the pressure singularity at the fracture front it is not possible to use traditional methods to track the free boundary evolution, which require an accurate velocity field that has to be derived from Poiseuille's Law which involves the derivative of the fluid pressure. Our numerical model uses a novel approach [12], known as the Implicit Level Set Algorithm (ILSA), to evolve

the fracture free boundary within each of the fracture planes. The distinguishing feature of this algorithm is its ability to locate the free boundaries of the fractures using the asymptotic behavior of the hydraulic fracture widths that are applicable at points in the neighborhood of the perimeters of the fractures. For the  $k^{\text{th}}$  fracture, the free boundary is located by the following iterative process: given initial guesses for each of the fracture boundaries  $\partial S_k$ , determine the corresponding equilibrating and volume conserving fracture widths  $w_k$  and fluid pressures  $p_{f,k}$ , and well-bore fluxes  $q_k$  subject to the constraints that the well-bore fluxes sum to the total fluid volume pumped and that the well-bore pressures are the same across the array. In the ribbons of elements that are completely filled with fluid and, which share at least one side with a partially filled tip element, use the trial width values to estimate the distance to the free boundary by inverting the applicable tip asymptotic behavior [11]; use these estimates of the distances to the free boundaries as initial conditions for the eikonal equations  $|\nabla T_k(x, y)| = 1$ , whose level set curves  $T_k(x, y) = 0$  define the free boundaries within the fracture planes. The fracture boundaries are then moved to the curves  $T_k(x, y) = 0$  and the iterative process is repeated until convergence is achieved. This algorithm can make use of the multi-scale hydraulic fracture tip asymptotic solution and is thus able to automatically capture the different types of propagation regimes with relatively coarse meshing of the fracture planes [13]. This iterative procedure is performed for each of the fractures in each of the fracture planes.

### 3. STRESS SHADOWING & INTERFERENCE FRACTURING

We illustrate these concepts by considering the evolution of the fractures in the five-fracture array that is depicted in Fig. 1. The parameters used in these illustrative examples are provided in section 4 below.

#### 3.1. Stress shadowing

If the spacing  $h_k$  between the perforation clusters is uniform, i.e.  $h_1 = h_2 = \dots = h_4$ , then, depending on the magnitude of the stage length  $Z$  relative to pay zone height  $H$  (see Fig. 1), the simultaneous propagation of fractures within the stage becomes susceptible to the phenomenon of stress shadowing [3-7]. Stress shadowing is characterized by the fracture growth within a stage being localized in the two outer, less constrained, fractures while there is minimal fracture growth within those fractures interior to the stage (see Fig. 2). This localization severely limits the total fractured area that can be achieved by the array of perforations. The total fractured area throughout the uniform array at the time  $t = 158$  s shown in Fig. 2 is  $3725 \text{ m}^2$ .

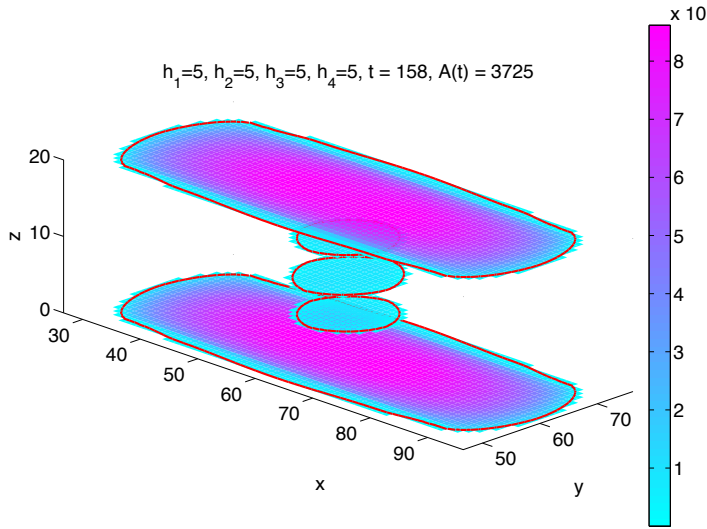


Fig. 2 Stress shadowing in a uniformly distributed array with  $Z = H = 20$  m, and  $h_k = 5$  m for all  $k=1, \dots, 4$ .

### 3.2. Interference fracturing

If, however, a non-uniform array is used, the dynamics of the mutual interaction between the simultaneously propagating fractures can be quite different [8]. In particular, if  $h_1 = 3.45$  m =  $h_4$  and  $h_2 = 6.55$  m =  $h_3$ , but otherwise if we use the same parameters that were used in the simulation shown in Fig. 2, then the so-called *interference fractures* 2 and 4 (using the numbering indicated in Fig.1) initially inhibit the runaway growth of the outer fractures 1 and 5 thereby allowing the middle fracture 3 to grow at almost the same rate as the outer fractures. After some time, the uptake of fluid switches from fractures 1, 3, and 5 to fractures 2 and 4. At this stage, fractures 2 and 4 cover a much smaller area than fractures 1, 3, and 5, however as a result of their increased uptake of fluid, new growth of fractures 2 and 4 starts to dominate fracture growth in the array. Indeed, the fracture opening at the well-bore in fractures 2 and 4 causes a displacement of the fluid away from the well-bore in fractures 1, 3, and 5 toward the perimeters of these fractures. This displacement of fluid away from the well-bore causes fractures 1, 3, and 5 to thin out and grow in extent in spite of the fact that they are, at this stage, accepting very little fluid from the well-bore. By the end of the simulation, the non-uniform array has the same volume as the uniform array but distributed among much thinner fractures that are spread over a much larger fractured area. The total fractured area throughout the non-uniform array at the time  $t = 158$  s is  $5561$  m<sup>2</sup> – an increase of 49% over the area generated by the uniform array with the same volume of fluid injected.

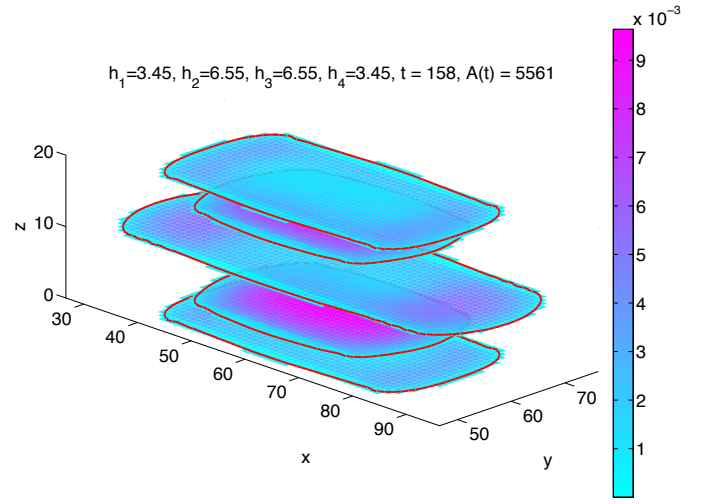


Fig. 3 Fracture development in a non-uniform array with  $Z = H = 20$  m and  $h_1 = 3.45$  m =  $h_4$  and  $h_2 = 6.5$  m =  $h_3$ .

## 4. NUMERICAL RESULTS

We explore the robustness of the interference fracturing process to structural changes in the configuration. We construct a one-parameter family of configurations by considering the five-fracture array shown in Fig. 1, which is subject to the constraints  $h_1 = h_4$  and  $h_2 = Z/2 - h_1 = h_3$ . By limiting ourselves to such symmetric perturbations to the uniform array we are able to explore the effect of structural changes to the configuration induced by varying the single parameter  $h_1$ .

### 4.1. Parameters for the numerical experiment

In all the experiments performed we used the following parameter set:

$$\begin{aligned}
 E &= 9.5 \text{ GPa}, & \nu &= 0.2, & K_{Ic} &= 0 \text{ MPa}\cdot\text{m}^{1/2} \\
 \mu &= 1 \text{ Pa}\cdot\text{s}, & Q_0 &= 0.1 \text{ m}^3 / \text{s}, & Z &= 20 \text{ m} \\
 \sigma_{zz}^0 &= 70 \text{ MPa}, & \Delta\sigma_{zz}^0 &= 5 \text{ MPa}, & H &= 20 \text{ m}
 \end{aligned}$$

Here  $E$  is the Young's modulus,  $\nu$  is the Poisson's ratio and  $K_{Ic}$  is the mode I material toughness for the elastic medium, which is assumed to be homogeneous;  $\mu$  is the dynamic viscosity of the fracturing fluid, which is assumed to be incompressible and Newtonian;  $Q_0$  is the total flux of fluid supplied to all the well-bores;  $Z$  and  $H$  are respectively the stage length and payzone height defined in Fig. 1. The well-bore is assumed to be straddled by a pair of symmetric stress barriers, located a distance  $H/2$  from the well-bore, across which the ambient geological confinement field  $\sigma_{zz}^0$  jumps by a constant amount  $\Delta\sigma_{zz}^0$  (see Fig. 1).

### 4.2. Regime of propagation

Since  $K_{Ic} = 0$ , we assume that the fractures in all the planes are propagating in the *viscosity dominated regime* [11], in which the viscous dissipation dominates the energy required to break the rock. If  $K_{Ic}$  were nonzero,

then this assumption would still be valid for example in the context of radially symmetric fractures provided:

$$t \ll \left( \frac{E'^{13} \mu'^5 Q_0^3}{K'^{18}} \right)^{1/2},$$

where  $E' = E/(1-\nu^2)$ ,  $\mu' = 12 \mu$ , and  $K' = (32/\pi)^{1/2} K_{Ic}$ .

### 4.3. Performance measures

In order to obtain a practical measure of the performance of a given configuration, which is associated with the interference fracture spacing  $h_I$ , we consider the total fractured area over all the fractures in the array up till time  $t$ , which we represent by  $A(t; h_I)$ . Since the total fractured area is related to the potential yield of hydrocarbons from the array, we will use  $A(t; h_I)$  as a measure of the efficacy of the hydraulic fracture treatment.

In order to obtain a measure of the cost of a given configuration we determine  $E(T; h_I)$  the total input energy expended throughout the fracturing process over the period  $[0, T]$ , which is given by:

$$E(T; h_I) = \int_0^T \sum_k p_k(t) q_k(t) dt = Q_0 \int_0^T p_1(t) dt \quad (1)$$

where the conditions

$$\sum_k q_k(t) = Q_0 \text{ and } p_k(t) = p_1(t)$$

have been used.

Finally, combining the yield and cost measures, we will consider the quotient  $A(T; h_I) / E(T; h_I)$ , which has units  $m^2/MJ$  and represents the total fractured area per unit of input energy for each configuration.

### 4.4. Performance variation with configuration

In Fig. 4 we plot the ratio  $A(T; h_I) / A(T; h_I=5)$  as a function of the configuration parameter  $h_I$ . This ratio represents the relative increase in the total fractured area that is achieved by decreasing  $h_I$  below  $h_I=5$ , which corresponds to the uniform configuration. Naturally, it is only feasible to perform such computationally intensive simulations for relatively few discrete values of  $h_I$ , which are depicted in the figure by the solid circles, while the intermediate values are obtained by interpolation. We observe that the uniform configuration, depicted in Fig. 2 with significant stress shadowing, corresponds to  $h_I=5$  m and a total fractured area of  $3725 \text{ m}^2$ . The optimal configuration depicted in Fig. 3, in which the interference fractures play a significant role, corresponds to  $h_I=3.45$  m and a total fractured area of  $5561 \text{ m}^2$ . As a measure of the robustness of this optimum, we observe the total fractured area can be increased by more than 40% by

selecting configurations for which  $h_I$  falls in the range:  $3.3 < h_I < 3.6$ .

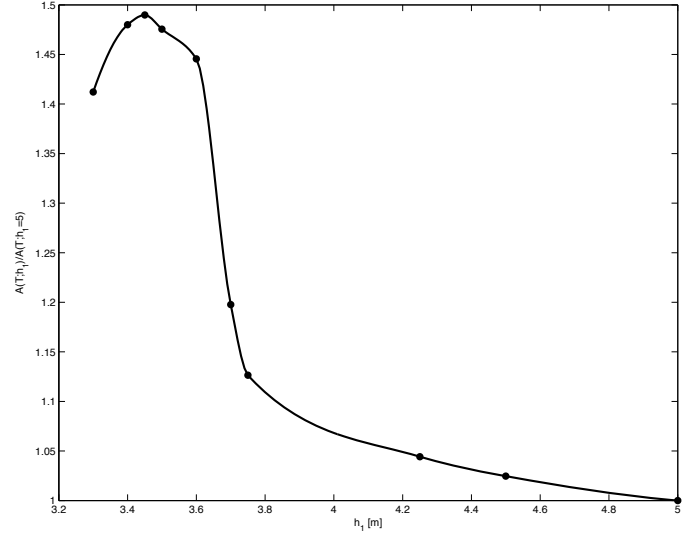


Fig. 4. The increase in the total fractured area  $A(T; h_I)$  relative to that of the uniform array for different values of  $h_I$  for the experimental five-fracture array with  $Z = H = 20$  m and  $h_1 = h_4$  and  $h_2 = Z/2 - h_1 = h_3$ .

In Fig. 5 we plot the total fractured area  $A(t; h_I)$  versus time  $t$  for a representative selection of values of the configuration perturbation parameter  $h_I$ . Initially, when all the fractures are small, so that their mutual interactions are insignificant, all configurations generate surface area at roughly the same rate. However, for  $t > 30$  s, the beneficial effect of the interference fractures can be clearly seen. For values of  $h_I$  in the neighborhood of the optimal configuration  $h_I = 3.45$  m, the generation of new fracture area occurs at approximately the same rate.

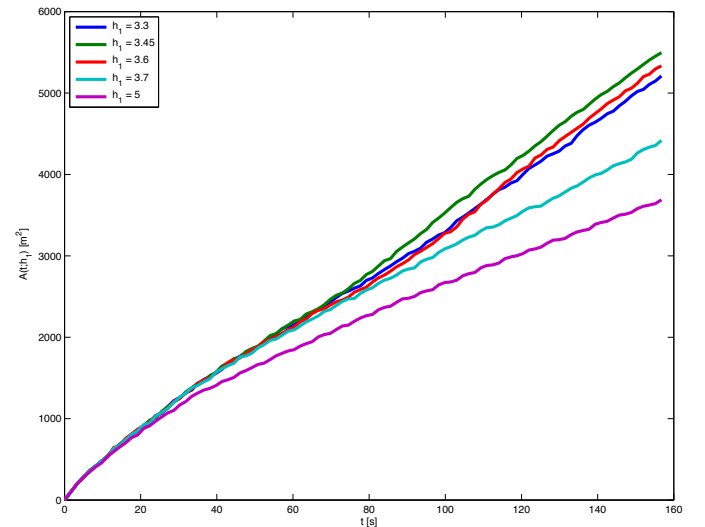


Fig. 5. The time evolution of the total fractured area  $A(t; h_I)$  for different values of  $h_I$  for the experimental five-fracture array.

In Fig. 6 we plot the time evolution of the well-bore pressure for the same selection of values of the

configuration perturbation parameter  $h_I$  and use the same color coding for the different values of  $h_I$  as was used in Fig. 5. The time traces of those well-bore pressures associated with effective interference fracturing all have significant changes in curvature with some exhibiting local maxima. In [8] it was shown that these local maxima correspond to the time after which the uptake of fluid by the interference fractures is dominant. Comparing Figs. 5 and 6, it can be seen that there is a significant change in the fracture area growth rate beyond this transition point. If the configuration parameter  $h_I$ , is reduced below the optimal value of 3.45 m to 3.3 m, it can be seen that local maximum is no longer present in the well-bore pressure plot.

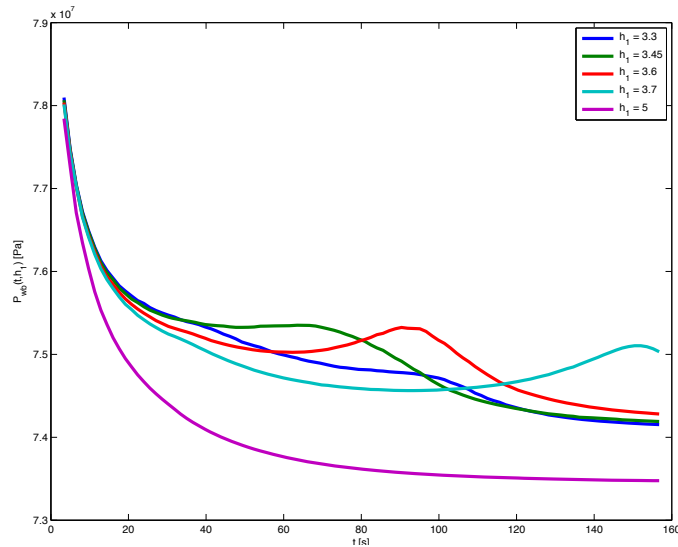


Fig. 6. The time evolution of the well-bore pressure  $P_{wb}(t; h_I)$  for different values of  $h_I$  for the experimental five-fracture array.

Integrating the well-bore pressures according to (1) we obtain the total input energy  $E(T; h_I)$ , which is plotted in Fig. 7 as a function of the configuration parameter  $h_I$ . It can be seen that the total input energy changes by less than 2% over the range of values of the configuration parameter  $h_I$  that were considered. Thus, it is anticipated that the increases in productivity indicated in Fig. 4 will come at little additional cost in terms of required energy input.

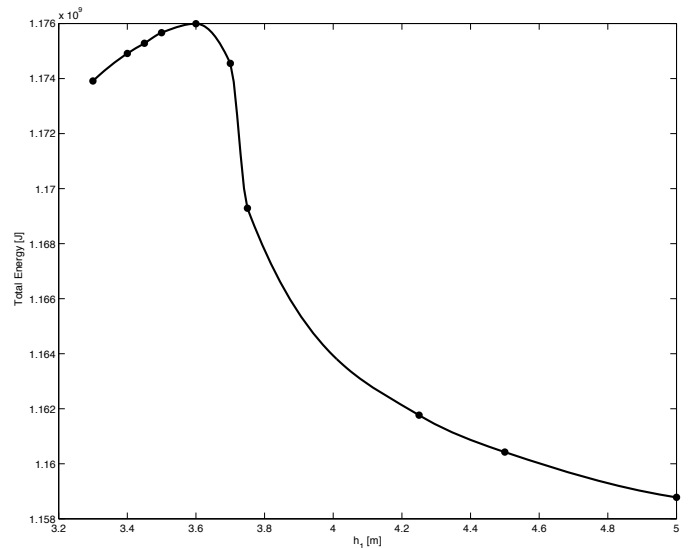


Fig. 7. The total input energy  $E(T; h_I)$  required to produce all the fractures in the five-fracture array for different values of the configuration parameter  $h_I$ .

To illustrate the cost effectiveness or efficiency of a given configuration, we plot the quotient  $A(T; h_I) / E(T; h_I) \times 10^6$  as a function of the configuration parameter  $h_I$  in Fig. 8. We observe that the shape of this curve is very similar to the area increase curve shown in Fig. 4. This is due to the fact that the total fracture energy is almost constant (changing by less than 2%) over the range of values of the configuration parameter considered.

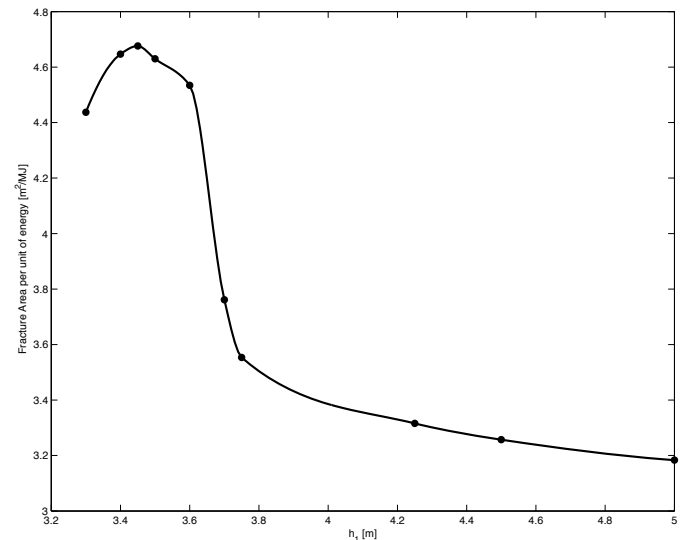


Fig. 8. The ratio  $A(T; h_I) / E(T; h_I) \times 10^6$  represents the efficiency, i.e.  $\text{m}^2$  of rock broken per MJ of energy expended, for the five-fracture array for different values of the configuration parameter  $h_I$ .

## 5. CONCLUSIONS

In this paper we have explored the robustness of the interference fracturing process as we sweep over a range of configurations. In order to be able to parameterize the changes in configuration, we considered a five-fracture array in which we restrict ourselves to symmetric perturbations of the interference fractures. We then monitored changes to various performance measures (e.g. increase in the total fractured area relative to a uniform array; total input energy required; fractured area generated per MJ of input energy) as we swept through different values of the one-parameter family of configurations.

For this experimental array we determined that it is possible to achieve increases in the generated fracture area of close to 50%, and increases of more than 40% can be achieved for a relatively broad range of values of the configuration parameter  $3.3 < h_f < 3.6$ . These potential gains in yield from a five-fracture array come at a less than 2% increase in the total energy input, which indicates the substantial potential benefits that can be derived by means of interference fracturing for negligible additional cost.

## REFERENCES

1. Bunger, A. P., Zhang, X., and Jeffrey, R. G. (In Press). Constraints on simultaneous growth of hydraulic fractures from multiple perforation clusters in horizontal wells. *Soc. Pet. Eng. J.*
2. Bunger, A.P and Peirce, A.P., Numerical Simulation of Simultaneous Growth of Multiple Interacting Hydraulic Fractures from Horizontal Wells, *Proc. ASCE Conf.*, Pittsburgh, 2014.
3. Germanovich, L. N., Ring, L. M., Astakhov, D. K., Shlyopobersky, J., and Mayerhofer, M. J. (1997). Hydraulic fracture with multiple segments II: Modeling. *Int. J. Rock Mech. Min. Sci.*, 34(3-4), 472.
4. Olson, J. E. (2004). Predicting fracture swarms – the influence of subcritical crack growth and the crack-tip process zone on joint spacing in rock. The initiation, propagation, and arrest of joints and other fractures, , J. W. Cosgrove and T. Engelder, eds., Geological Society, London, vol. 231, 73–87.
5. Fisher, M. K., Heinze, J. R., Harris, C. D., Davidson, B. M., Wright, C. A., and Dunn, K. P. (2004). Optimizing horizontal completion techniques in the barnett shale using microseismic fracture mapping. Proceedings SPE Annual Technology Conference and Exhibition, Houston, Texas, USA. SPE 90051.
6. Abass, H. H., Soliman, M. Y., Tahini, A. M., Surjaatmadja, J., Meadows, D. L., and Sierra, L. (2009). Oriented fracturing: A new technique to hydraulically fracture an openhole horizontal well. Proceedings SPE Annual Technical Conference and Exhibition, New Orleans, LA, USA. SPE 124483.
7. Meyer, B. and Bazan, L. (2011). A discrete fracture network model for hydraulically induced fractures-theory, parametric and case studies. Proceedings SPE Hydraulic Fracturing Technology Conference and Exhibition, The Woodlands, Texas, USA. SPE 140514.
8. Peirce, A. P. and Bunger, A. P. (Under Review). Interference fracturing: Non-uniform distributions of perforation clusters that promote simultaneous growth of multiple hydraulic fractures. *Soc. Pet. Eng. J.* pre-print available at: <http://hdl.handle.net/2429/45492>.
9. Crouch, S.L. and A.M. Starfield. 1983. *Boundary element methods in solid mechanics*. 1<sup>st</sup> ed. London: George Allen & Unwin.
10. Detournay E. and Peirce A.P., On the Moving Boundary Conditions for a Hydraulic Fracture, *Int. J. of Eng. Sci.*, (accepted for publication, December 2013).
11. Detournay, E. 2004. Propagation regimes of fluid-driven fractures in impermeable rocks. *Int. J. Geomechanics* volume 4 (1): 1–11.
12. Peirce, A. and Detournay, E. (2008). An implicit level set method for modeling hydraulically driven fractures. *Computer Meth. Appl. Mech. Eng.*, 197, 2858–2885.
13. Lecampion B., Peirce A.P, Detournay E., Zhang X., Chen Z., Bunger A.P., Detournay C., Napier J., Abbas S., Garagash D., Cundall, P., 2013. The impact of the Near-Tip Logic on the Accuracy and Convergence Rate of Hydraulic Fracture Simulators Compared to Reference solutions. In: *Effective and Sustainable Hydraulic Fracturing*, AP Bunger, J McLennan and R Jeffrey (eds.), ISBN 978-953-51-1137-5, (Intech), Chapter 43, p 855-873.